Iranian Journal of Numerical Analysis and Optimization
Vol. 10, No. 2, (2020), pp 177–196
DOI:10.22067/ijnao.v10i2.86296

Research Article

Numerical solution of the Allen–Cahn equation by using "shifted" surface spline radial basis functions

C.G. Keshavarzi and F. Ghoreishi*

Abstract

We consider a fully-discrete approximation of the Allen–Cahn equation, such that the forward Euler/Crank–Nicolson scheme (in time) combined with the RBF collocation method based on "shifted" surface spline (in space). Numerical solvability and stability of the method, by using second order finite difference matrices are discussed. We show that, in the proposed scheme, the nonlinear term can be treated explicitly and the resultant numerical scheme is linear and easy to implement. Numerical results that show the efficiency and reliability of the proposed method are presented, and two types of collocation nodes for solving this equation are compared.

AMS(2010): Primary 65N35; Secondary 65L07.

Keywords: Allen–Cahn equation; RBF collocation method; Shifted surface spline; Stability; Solvability.

1 Introduction

The radial basis function method is one of the most useful tools for interpolating multidimensional scattered data. The method has remarkable properties, to handle arbitrarily scattered data, to adjust to several space dimensions easily, and to provide powerful convergence properties, which have made it popular in sciences and mathematics; see [16, 26, 6, 28]. Some of the more

*Corresponding author
Received 6 April 2020; revised 16 May 2020; accepted 20 August 2020

Changiz Goli Keshavarzi
Department of Mathematics, K. N. Toosi University of Technology, Tehran, Iran. e-mail: ckeshavarzi@mail.kntu.ac.ir.

Farideh Ghoreishi
Department of Mathematics, K. N. Toosi University of Technology, Tehran, Iran. e-mail: ghoreishif@kntu.ac.ir

recent applications of radial basis functions include measurements of potential or temperature on the earth's surface [3], mathematical finance [11], data mining [19], neural network [18], tomographic reconstruction, medical imaging [4], and the numerical solution of partial differential equations (PDEs).

The Allen–Cahn equation was initially introduced by Allen and Cahn [1] in 1979 for antiphase domain coarsening in a binary alloy. This equation, as the simplest model of phase-field, describes the evaluation of diffuse phase boundary, concentrated in a small region. It is known that the Allen–Cahn equation is well-posed and has a unique solution that satisfies the maximum principle; see [12]. The Allen–Cahn equation has been widely used in many complicated moving interface problems in fluid dynamics and material science applications, such as crystal growth [7] and tumor growth [27] on flat surfaces.

During the past two decades, a great deal of mathematical efforts have been devoted to the study of numerical solution for the Allen–Cahn equation [20, 31, 12], and finite difference [13], finite element [9], Fourier spectral with periodic boundary condition [15], and RBF methods[17] are some of the recently proposed methods.

In this paper, a fully-discrete approximation of the Allen–Cahn equation is considered, such that a first order (Euler/Crank–Nicolson) finite difference scheme (in time) combined with the RBF collocation method (in space). Here, the main goal is how to construct an efficient numerical scheme based on the RBF collocation method that preserves the maximum principle and energy dissipation law in the Allen–Cahn equation. We will use a special kind of RBFs as the shifted surface splines [8, 29, 28, 30]. These functions include all of the multiquadric, thin plate, and power RBFs, which their properties quite well understood, theoretically and practically [3, 8, 26]. For example, some features of multiquadric, thin plate, and power RBFs are as follows:

• Multiquadrics are strictly positive definite, but surface splines and powers are conditionally positive definite.

• Powers and surface splines give an algebraic rate of convergence, but multiquadrics can achieve spectral rate of convergence.

• Multiquadrics interpolation is always solvable, provided that the points are disjoint, but for surface splines and powers, for solvability, we need to add some appropriate number of functions (polynomials). It is worth noting the shifted surface spline $(-1)^{m-s/2+1}\left(x^2+\delta^2\right)^{m-s/2}\log\left(x^2+\delta^2\right)^{1/2}$, where s is even and $\delta \neq 0$, is strictly conditionally positive definite (see [3, p. 104]). Hence, for the well-posedness of the interpolation problem, we need to add some appropriate polynomial to this function.

• Powers and surface splines are piecewise smooth, but multiqudrics are infinitely smooth.

• Franke's research [10] showed that multiquadrics, in terms of simplicity of implementation, stability, and accuracy, have much better performance among 29 available interpolation methods used for interpolating two-dimensional analytic functions.

In the proposed scheme, the nonlinear term can be treated explicitly such that, the resultant numerical scheme will be linear and easy to implement. The numerical solvability and stability of the method by using the RBF-FD procedure based on the classical finite difference method are discussed. The RBF-FD method uses the simplicity of FDM formulation and the meshfree property of RBFs, which was proposed in [22, 21]. Also, Tolstykh, Lipavskii, and Shirobokov [24] and Wright and Fornberg [25] introduced this method independently for the numerical approximation of the ODEs and PDEs. For flat RBF, Wright and Fornberg [25] showed that the RBF-FD scheme is the same as the conventional finite difference scheme. The RBF-FD method is used with other names such as local radial basis function method [23] and local radial basis functions based on the differential quadrature method. By using some numerical experiments, we show that the proposed method with equally spaced collocation nodes may give better results in comparison with scattered nodes.

The paper is organized as follows. In Section 2, the RBF interpolation is introduced in brief. Section 3 reviews the RBF collocation methods. In Section 4, numerical results that show the efficiency of the proposed method are given. The last section ends with concluding remarks.

2 The RBF interpolation method

Before we pose the RBF interpolation, we need to recall the following definitions.

Definition 1. A continuous and even function $f : \mathbb{R}^d \to \mathbb{R}$ is said to be strictly conditionally positive definite of order k (SCPD(k)) if, for all $N \in \mathbb{N}$, all sets $\chi = \{X_0, \ldots, X_N\} \subset \mathbb{R}^d$, and all $\lambda \in \mathbb{R}^N$ satisfying

$$\sum_{i=0}^{N} \lambda_i q\left(X_i\right) = 0,$$

for all real-valued polynomials q of degree less than k, the quadratic form

$$\lambda^t A \lambda = \sum_{i=0}^{N} \sum_{j=0}^{N} \lambda_i \lambda_j f\left(\|X_i - X_j\|\right),$$

is positive, unless λ is zero.

Let $\Pi_k\left(\mathbb{R}^d\right)$ be the space of d-variate polynomials of degree at most k; then we have the following definition.

Definition 2. A set of distinct points $\{X_0, \ldots, X_N\}$ in $\mathbb{R}^d$ is said to be

$\Pi_k\left(\mathbb{R}^d\right)$-unisolvent if the only element of $\Pi_k\left(\mathbb{R}^d\right)$ that vanishes at each x_i is the zero polynomial.

The definition of multivariate RBF interpolation can be stated as follows:

Definition 3. Given a set $\chi = \{X_i\}_{i=0}^N$ of distinct centers in $\mathbb{R}^d$ and a target function $v : \mathbb{R}^d \to \mathbb{R}$, the RBF interpolant is given by

$$Sv\left(X\right) = \sum_{j=0}^{N} \lambda_j \phi\left(\|X - X_j\|\right) + \sum_{k=0}^{M} \gamma_k p_k\left(X\right), \quad M \leq N, \tag{1}$$

where $\phi\left(\|X - X_j\|\right)$ is a strictly conditionally positive definite RBF of order m, centered on the points x_j, and $\{p_k\left(X\right)\}_{k=0}^M$ forms a basis for the polynomial space $\Pi_{m-1}\left(\mathbb{R}^d\right)$, where $M = \binom{d+m-1}{m-1}$. The expansion coefficient λ_j, γ_k are determined by the interpolation conditions,

$$Sv\left(X_j\right) = v\left(X_j\right), \quad 0 \leq j \leq N,$$

and the following additional conditions are considered to handle the additional degree of freedom

$$\sum_{j=0}^{N} \lambda_j p_k\left(X_j\right) = 0, \quad 0 \leq k \leq M.$$

These conditions lead to a system of equations that can be written down in the matrix form as

$$\begin{pmatrix} \Phi & P \\ P^t & 0 \end{pmatrix} \begin{pmatrix} \boldsymbol{\lambda} \\ \boldsymbol{\gamma} \end{pmatrix} = \begin{pmatrix} V \\ 0 \end{pmatrix}, \tag{2}$$

where

$$\Phi_{ij} = \phi\left(\|X_i - X_j\|\right), \;\; P_{ij} = p_j\left(X_i\right), \;\; \boldsymbol{\lambda} = \left(\lambda_0, \ldots, \lambda_N\right)^t,$$
$$\boldsymbol{\gamma} = \left(\gamma_0, \ldots, \gamma_M\right)^t, \;\; V = \left(v_0, \ldots, v_N\right)^t.$$

As it is shown in [26] that system (2) is uniquely solvable when ϕ is strictly conditionally positive definite of order m and χ is $\Pi_{m-1}\left(\mathbb{R}^d\right)$-unisolvent set of centers; so the coefficient matrix in (2) is invertible.

In this paper, we use "shifted" surface splines as radial basis functions ϕ, which include the multiquadric and thin plate spline and are defined as follows:

$$\phi_\delta\left(x\right) := \begin{cases} (-1)^{\lceil m - s/2 \rceil} \left(x^2 + \delta^2\right)^{m - s/2}, & s \text{ is odd}, \\ (-1)^{m - s/2 + 1} \left(x^2 + \delta^2\right)^{m - s/2} \log\left(x^2 + \delta^2\right)^{1/2}, & s \text{ is even}, \end{cases}$$

where s, $m \in N$, $m > s/2$ and $\lceil s \rceil$ indicates the smallest integer greater than s. For odd s, ϕ_δ is called the multiquadric RBF, and for $\delta = 0$, the function ϕ_δ is called the surface spline.

In what follows, we consider the number h as the "density" of $\chi = \{X_0, \ldots, X_N\}$ in Ω, as follows:

$$h = h(\Omega; \chi) := \sup_{X \in \Omega} \min_{X_k \in \chi} |X - X_k| .$$

3 The RBF collocation method, stability and numerical solvability

In this section, we use the forward Euler/Crank–Nicolson scheme for the time and classical RBF method for spatial discretization in numerical approximation of the Allen–Cahn equation. Let us define $t_k = k * \tau, k = 0, 1, \ldots, \mathcal{M}$, where $\tau = \frac{T}{\mathcal{M}}$ and $\mathcal{M}$ is the number of the time steps. we introduce notations $v_j(X) = v(X, t_j)$ and $\partial_t v_j = \frac{v_{j+1} - v_j}{\tau}$. Also we define $\widehat{v}_j = \frac{v_{j+1} + v_j}{2}$.

Consider the following time-dependent Allen–Cahn equation:

$$\begin{cases} \frac{\partial v(X,t)}{\partial t} - \Delta v(X,t) + \frac{1}{\eta^2} f(v(X,t)) = 0, & X \in \Omega \subset \mathbb{R}^d, t \in [0,T] \\ v(X,t) = g(X), & X \in \partial\Omega, \end{cases} \tag{3}$$

which is supplemented with the following initial condition:

$$v(X,0) = v_0(X) \quad in\, \Omega,$$

where Ω is a bounded convex domain with Lipschitz boundary $\partial\Omega$, $T > 0$ is a positive constant, and $f(v) = v^3 - v$ is the reaction term with $F(v) = \frac{1}{4}(v^2 - 1)^2$, a given energy potential that drives the solution into the two pure states $v = \pm 1$. The nonlinearity $f(v)$ is monotone outside the interval $[-1, 1]$, so solutions of the Allen–Cahn equation satisfy a maximum principle; see [12, 2]. Also, $g(X)$ and $X \in \partial\Omega$ are known constants. The parameter η, which usually stands for the inter-facial width, is a small constant compared to the characteristic length of the laboratory scale. The function $v(X,t)$ is a distribution function of the concentration for one of the two metallic components of the alloy.

In the RBF collocation method, the solution $v(X,t)$ is approximated by a linear combination of RBFs as

$$v_N(X,t) = \sum_{j=0}^{N} \lambda_j(t)\, \phi(\|X - X_j\|) + \sum_{k=0}^{M} \gamma_k(t)\, p_k(X), \; M \le N, \tag{4}$$

where ϕ and $p_k(X)$ are defined in (1). The collocation points $\{X_i\}_{i=0}^{N}$ has been selected in such a way that $\{X_0, \ldots, X_{N_I}\} \subset \Omega$ and $\{X_{N_I+1}, \ldots, X_N\} \subset \partial\Omega$. In RBF collocation method, the requirement is that (3) is satisfied exactly by (4) at the following relations.

$$\frac{\partial v_N\left(X_k,t\right)}{\partial t}-\Delta v_N\left(X_k,t\right)+\frac{1}{\eta^2}f\left(v_N\left(X_k,t\right)\right)=0,\quad k=0,1,\ldots,N_I,$$
$$v_N\left(X_k,t\right)=g(X_k),\qquad k=N_I+1,\ldots,N,$$

and the initial conditions are

$$v_N\left(X_k,0\right)=v_0,\ \ k=0,1,\ldots,N.$$

According to the forward Euler/Crank–Nicolson scheme in time, we discretize the Allen–Cahn equation as follows:

$$\frac{v_N\left(X_k,t_{j+1}\right)-v_N\left(X_k,t_j\right)}{\tau}-\frac{\Delta v_N\left(X_k,t_{j+1}\right)+\Delta v_N\left(X_k,t_j\right)}{2}$$
$$+\frac{1}{\eta^2}f\left(v_N\left(X_k,t_j\right)\right)=0,\quad k=0,1,\ldots,N,$$

where τ is a mesh size in time and $X_k=\left(x_i,y_l\right),i,l=0,\ldots,n$, with $N=(n+1)^2-1$. Equivalently,

$$\left(v_N\right)_k^{j+1}-\frac{\tau}{2}(\Delta v_N)_k^{j+1}=\left(v_N\right)_k^j+\frac{\tau}{2}(\Delta v_N)_k^j$$
$$-\frac{\tau}{\eta^2}f\left(\left(v_N\right)_k^j\right)=0,\ \ k=0,1,\ldots,N \tag{5}$$

where

$$\left(v_N\right)_k^j=v_N\left(X_k,t_j\right),\quad (\Delta v_N)_k^j=\Delta v_N\left(X_k,t_j\right)=\left(\left(v_N\right)_{xx}+\left(v_N\right)_{yy}\right)_k^j.$$

In addition, we impose the following constraints,

$$\sum_{j=0}^{N}\lambda_j\left(t\right)p_i\left(X_j\right)=0,\quad 0\leqslant i\leqslant M. \tag{6}$$

From (5) and (6), we have a system with $N+M+2$ unknowns $\{\lambda_k\}_{k=0}^N$ and $\{\gamma_k\}_{k=0}^M$ and $N+M+2$ equations. But, before imposing boundary conditions, we will simplify systems (5) and (6), by using finite difference matrices.

Now, If we set $\Phi_{ik}=\phi(\|X_i-X_k\|)$ and $\Delta\Phi_{ik}=\Delta\phi(\|X_i-X_k\|)$, then we can rewrite collocation equation (5) and (6) in the matrix notation as

$$\left[\begin{pmatrix}\Phi & P\\ P^t & 0\end{pmatrix}-\frac{\tau}{2}\begin{pmatrix}\Delta\Phi & \Delta P\\ P^t & 0\end{pmatrix}\right]\Lambda^{j+1}=\frac{\tau}{\eta^2}\begin{pmatrix}-f((v_N)_k^j)\\ 0\end{pmatrix}$$
$$+\begin{pmatrix}\frac{\tau}{2}\Delta\left(v_N\right)_k^j+\left(v_N\right)_k^j\\ 0\end{pmatrix}, \tag{7}$$

where $\Lambda^{j+1}=\begin{pmatrix}\boldsymbol{\lambda}^{j+1}\\ \boldsymbol{\gamma}^{j+1}\end{pmatrix}$. Now, by using (2), we may write (7) as

$$\left[\begin{pmatrix} \Phi & P \\ P^t & 0 \end{pmatrix} - \frac{\tau}{2}\begin{pmatrix} \Delta\Phi & \Delta P \\ P^t & 0 \end{pmatrix}\right] A^{-1}\begin{pmatrix} V^{j+1} \\ 0 \end{pmatrix} = -\frac{\tau}{\eta^2}\begin{pmatrix} f((v_N)_k^j) \\ 0 \end{pmatrix} + \begin{pmatrix} \frac{\tau}{2}\Delta\,(v_N)_k^j + (v_N)_k^j \\ 0 \end{pmatrix}, \tag{8}$$

where $V^l = [(v_N)_0^l, (v_N)_1^l, \ldots, (v_N)_N^l]^t, l = 0, \ldots, \mathcal{M}$ and

$$A = \begin{pmatrix} \Phi & P \\ P^t & 0 \end{pmatrix},$$

which is a dense linear system and when solved, we obtain an RBF based on the numerical approximation for (3). However, for a stable computation, we have to consider, stability issues for time-dependent problems and adapt the proposed method for nonlinear equations.

To obtain stability criterion for system (8), we will use a recently proposed local method that causes more flexibility for handling nonlinearities. In this method, essentially a classical finite difference (FD) method or generalization of them to scattered node layouts are considered, which is known as RBF-FD methods. This kind of methods have been investigated independently by Shu et al. [22, 21], Tolstykh, Lipavskii, and Shirobokov [24], Cecil, Qian, and Osher [5], Wright and Fornberg [25]. Here, we only consider its most general form, in which, the FD method consists of approximating second order derivative of base functions at a given point, based on a linear combination of the value of radial basis functions at some surrounding nodes. In other words, we will use a classical 2-dimensional case as follows:

$$\frac{d^2}{dx^2}\phi_s\left(\|X\|\right)|_{x=x_j} \backsimeq \sum_{i=0}^{k} w_{j,i}^{(2)}\phi_s\left(\|X_i\|\right), \quad 0 \le j \le n, \quad 1 \le k \le n,$$

where $w_{i,j}^{(2)}$ is called the FD weights and $\phi_s\left(\|X\|\right) = \phi\left(\|X - X_s\|\right)$. This formula can be combined to create FD formulas for partial derivatives in two and higher dimensions. In classical central finite difference approximation of order two, FD weights can be considered as:

$$\begin{aligned}\frac{d^2}{dx^2}\phi_s\left(\|X\|\right)|_{x=x_j} &\backsimeq \sum_{i=0}^{k} w_{j,i}^{(2)}\phi\left(\|X_i\|\right) \\ &= \frac{\phi\left(\|X_{j+1}\|\right) - 2\phi\left(\|X_j\|\right) + \phi_s\left(\|X_{j-1}\|\right)}{h^2},\end{aligned}$$

where h is the spatial distance of nodes. In two-dimensional case, we have

$$\begin{aligned}\frac{d^2}{dx^2}\phi_s\left(\|X\|\right)|_{x=x_j} + \frac{d^2}{dy^2}\phi_s\left(\|X\|\right)|_{y=y_i} \backsimeq{}& \frac{\phi_s\left(\|X_{j+1,i}\|\right) - 2\phi_s\left(\|X_{j,i}\|\right) + \phi_s\left(\|X_{j-1,i}\|\right)}{h^2} \\ &+ \frac{\phi_s\left(\|X_{j,i-1}\|\right) - 2\phi_s\left(\|X_{j,i}\|\right) + \phi_s\left(\|X_{j,i-1}\|\right)}{h^2}.\end{aligned}$$

In the matrix notation, we may write $\Delta\Phi = \frac{1}{h^2}F^{(2)}\Phi$, where the finite difference matrix $F^{(2)}$ is as follows:

$$F^{(2)} = \begin{pmatrix} -4 & 1 & 0 & \dots & 0 & 1 & 0 & 0 & \dots \\ 1 & 0 & 0 & & 1 & -4 & 1 & 0 & \\ 0 & 0 & 0 & \dots & 0 & 1 & 0 & 0 & \dots \\ \vdots & \vdots & \vdots & \vdots & \vdots & \vdots & \vdots & \vdots & \\ 0 & 0 & 0 & \dots & 0 & 0 & 0 & 0 & \dots \\ 1 & -4 & 1 & & 0 & 0 & 1 & 0 & \\ 0 & 1 & 0 & \dots & 0 & 1 & -4 & 1 & \dots \\ \vdots & & \vdots & & \vdots & & \vdots & & \ddots \end{pmatrix}.$$

From $\Delta\Phi = \frac{1}{h^2}F^{(2)}\Phi$ and $\Delta P = \frac{1}{h^2}F^{(2)}P$, collocation equation (8) can be written as

$$\left[\begin{pmatrix} \Phi & P \\ P^t & 0 \end{pmatrix} - \frac{\tau}{2h^2}\begin{pmatrix} F^{(2)} & 0 \\ 0 & I \end{pmatrix}\cdot\begin{pmatrix} \Phi & P \\ P^t & 0 \end{pmatrix}\right] A^{-1}\begin{pmatrix} V^{j+1} \\ 0 \end{pmatrix} = R, \qquad (9)$$

where R is the right-hand side of (8). For example, for $n = 2, (N = (n+1)^2)$, we have

$$F^{(2)} = \begin{pmatrix} -4 & 1 & 0 & 1 & 0 & 0 & 0 & 0 & 0 \\ 1 & 0 & 1 & -4 & 1 & 0 & 1 & 0 & 0 \\ 0 & 0 & 0 & 1 & 0 & 1 & -4 & 1 & 0 \\ 1 & -4 & 1 & 0 & 1 & 0 & 0 & 0 & 0 \\ 0 & 1 & 0 & 1 & -4 & 1 & 0 & 1 & 0 \\ 0 & 0 & 0 & 0 & 1 & 0 & 1 & -4 & 1 \\ 0 & 1 & -4 & 1 & 0 & 1 & 0 & 0 & 0 \\ 0 & 0 & 1 & 0 & 1 & -4 & 1 & 0 & 1 \\ 0 & 0 & 0 & 0 & 0 & 1 & 0 & 1 & -4 \end{pmatrix}.$$

Now, (9) can be written equivalently as

$$\left[I_{N+1} - \frac{\tau}{2h^2}F^{(2)}\right]V^{j+1} = \left[-\frac{\tau}{\eta^2}f((v_N)_k^j) + \frac{\tau}{2}\Delta(v_N)_k^j + (v_N)_k^j\right]_{k=0}^{N}. \qquad (10)$$

It is well known that the eigenvalues of $F_{xx}^{(2)}$ $\left(F_{yy}^{(2)}\right)$ are $\lambda_i = -4\sin^2(\frac{i\pi}{2(N+1)})$, or $\rho(F^{(2)}) \leq 8$, that is, $\mid 1 - \frac{4\tau}{h^2} \mid \leq 1$. Hence for a stable computation, we need $\frac{2\tau}{h^2} \leq 1$.

Note that the eigenvalues of $F^{(2)}$ after imposing boundary conditions are less than or equal to zero. Therefore, $1 - \frac{\tau\lambda_i}{2h^2} \neq 0$ for all $0 \leq i \leq N$. Thus, clearly system (10) is numerically solvable.

According to considered order of mesh points $\{x_i, y_j\}$,

$$\{\{x_0, y_0\}, \{x_0, y_1\}, \dots, \{x_0, y_n\}, \{x_1, y_0\}, \{x_1, y_1\}, \dots, \{x_1, y_n\}, \dots, \{x_n, y_n\}\}$$

and given boundary conditions on x_0, x_n, y_0, y_n, system (8) after imposing boundary conditions is completed. This is a system with $N+1$ unknowns and equations. Therefore, after imposing given boundary conditions, (8) can be solved directly, by using stability condition $\frac{2\tau}{h^2} \leq 1$.

4 Numerical illustrations

In this section, we present four numerical examples to illustrate the accuracy and efficiency of the proposed scheme. According to our observations, when equally spaced nodes are used as a set of collocation points, we obtain better results in comparison with scattered mesh points. In all of test problems, we have used multiquadratic radial basis functions with $\tau \leq \eta^2$ and $\tau \leq h^2/2$. In Example 1, the standard surface spline is considered too. For comparison, at time $t = T$, the infinity norm of the error

$$\|v - Sv\|_\infty = \max_{1 \leq i \leq N} |v(X_i, T) - Sv(X_i, T)|,$$

and the root mean square (RMS) norm of the error

$$\|v - Sv\|_2 = \sqrt{\frac{1}{N} \sum_{i=1}^{N} (v(X_i, T) - Sv(X_i, T))^2},$$

are used, where N is the number of collocation points.

Example 1. Consider two-dimensional Allen–Cahn equation with the following initial and boundary conditions:

$$\begin{cases} \dfrac{\partial v}{\partial t} - \Delta v + \dfrac{1}{\eta^2}(v^3 - v) = f, \ \ (x, y) \in (-1, 1)^2, \ t > 0, \\ v(\pm 1, y, t) = 0, \ v(x, \pm 1, t) = 0, \ t > 0, \\ v(x, y, 0) = 0, \ \ (x, y) \in [-1, 1]^2, \end{cases}$$

where $\eta = 100$, the exact solution is $v(x, y, t) = \tanh\left(\left(x^2 - 1\right)\left(y^2 - 1\right)t\right)$ and the function f is computed accordingly.

In this example, we apply the proposed method by using two types of nodes. As shown in Table 1, the obtained errors for equally spaced nodes are slightly better than scattered nodes. We plot the absolute error of this example in Figure 1 and the contour plot of the error in Figure 2. The comparison of errors of Example 1 by using different time steps for $t = 1000\tau$ at $N = 100$ is presented in Table 2.

Table 1: The comparison of errors of Example 1, by considering "shifted" surface spline, at $t = 1000\tau$ by using scattered and equally spaced nodes where time step is $\tau = 10^{-4}$.

	Equally Spaced		Scattered	
N	$\|u - u_N\|_\infty$	$\|u - u_N\|_2$	$\|u - u_N\|_\infty$	$\|u - u_N\|_2$
49	$4.82043E-6$	$1.41187E-5$	$4.26723E-6$	$1.30836E-5$
64	$4.07495E-6$	$1.33603E-5$	$3.35978E-6$	$1.34205E-5$
81	$1.31830E-6$	$5.20152E-6$	$7.72547E-7$	$3.28669E-6$
100	$1.12669E-6$	$5.04211E-6$	$7.65370E-7$	$2.91935E-6$
121	$7.02509E-7$	$3.32090E-6$	$7.56430E-7$	$1.94812E-6$
144	$6.73415E-7$	$3.52046E-6$	$6.22881E-7$	$2.15101E-6$

Table 2: The comparison of errors of Example 1, by using various time steps at $N = 100$ and $t = 1000\tau$.

	Equally Spaced		Scattered	
Time Step ($\tau = 10^{-4}$)	$\|u - u_N\|_\infty$	$\|u - u_N\|_2$	$\|u - u_N\|_\infty$	$\|u - u_N\|_2$
τ	$1.12669E-6$	$5.04211E-6$	$7.65370E-7$	$2.91935E-6$
$1/2 \times \tau$	$2.78156E-7$	$1.17651E-6$	$1.33866E-7$	$6.79208E-7$
$1/4 \times \tau$	$6.91386E-8$	$2.85469E-7$	$3.36881E-8$	$1.65689E-7$
$1/8 \times \tau$	$1.72370E-8$	$7.04178E-8$	$8.64618E-9$	$4.10731E-8$
$1/16 \times \tau$	$4.30344E-9$	$1.74946E-8$	$2.19114E-9$	$1.02357E-8$

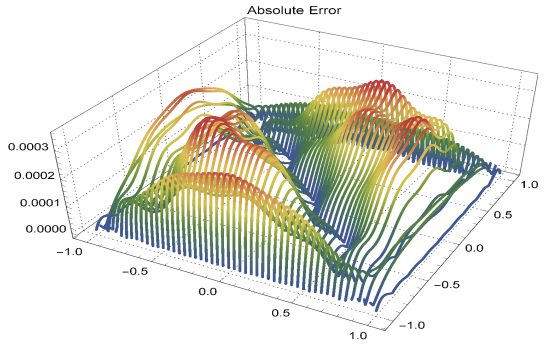

Figure 1: The plot of the absolute error in Example 1, at $t = 1000\tau$ and $N = 100$ with equally spaced nodes.

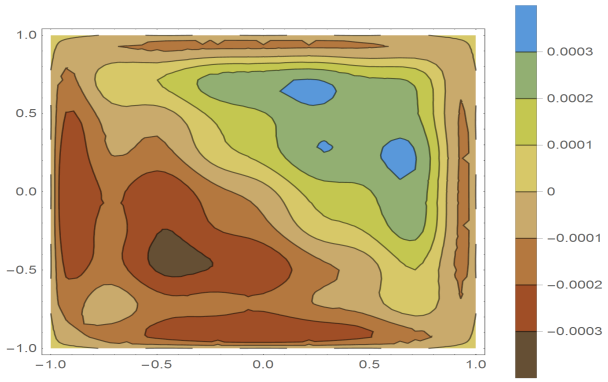

Figure 2: The contour plot of the error in Example 1, at $t = 1000\tau$ and $N = 100$ with equally spaced nodes.

In what follows, we solve Example 1, by considering the standard surface spline $\phi(r) = r^2 \log r$. Comparing the results obtained in Tables 1–4, it can be seen that the "shifted" surface spline provides better results than the standard surface spline. The absolute error and contour plot of the error, for this case, is plotted in Figures 1 and 4, respectively.

Table 3: The comparison of errors of Example 1, by considering standard surface spline, at $t = 1000\tau$ by using scattered and equally spaced nodes where time step is $\tau = 10^{-4}$.

Equally Spaced			Scattered	
N	$\|u - u_N\|_\infty$	$\|u - u_N\|_2$	$\|u - u_N\|_\infty$	$\|u - u_N\|_2$
49	$6.51165E-6$	$1.84565E-5$	$5.57870E-6$	$1.78168E-5$
64	$5.59294E-6$	$1.74854E-5$	$4.96732E-6$	$1.79523E-5$
81	$1.84662E-6$	$6.64194E-6$	$1.13404E-6$	$4.34977E-6$
100	$1.58833E-6$	$6.32184E-6$	$8.10437E-7$	$3.54860E-6$
121	$7.04900E-7$	$3.59848E-6$	$7.72250E-7$	$1.96949E-6$
144	$6.74292E-7$	$3.73803E-6$	$6.20674E-7$	$2.14926E-6$

Table 4: The comparison of errors of Example 1, by considering standard surface spline, by using various time steps at $N = 100$ and $t = 1000\tau$.

Equally Spaced			Scattered	
Time Step ($\tau = 10^{-4}$)	$\|u - u_N\|_\infty$	$\|u - u_N\|_2$	$\|u - u_N\|_\infty$	$\|u - u_N\|_2$
τ	$1.58833E-6$	$6.32184E-6$	$8.10437E-7$	$3.54860E-6$
$1/2 \times \tau$	$3.91406E-7$	$1.50928E-6$	$1.85967E-7$	$8.74747E-7$
$1/4 \times \tau$	$9.71936E-8$	$3.69865E-7$	$5.01409E-8$	$2.20779E-7$
$1/8 \times \tau$	$2.42193E-8$	$9.16348E-8$	$1.30555E-8$	$5.57276E-7$
$1/16 \times \tau$	$6.04515E-9$	$2.28113E-8$	$3.33334E-9$	$1.40169E-8$

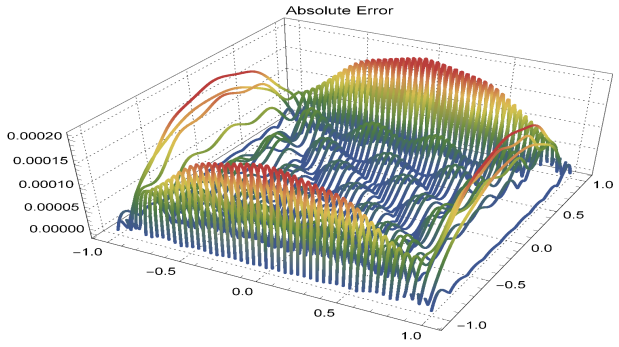

Figure 3: The plot of the absolute error in Example 1, by considering the standard surface spline, at $t = 1000\tau$ and $N = 100$ with equally spaced nodes.

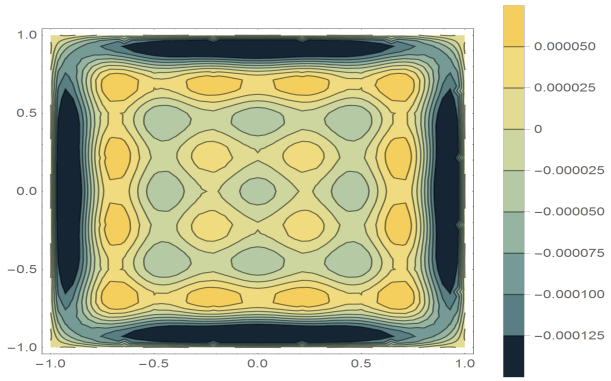

Figure 4: The contour plot of the error in Example 1, by considering the standard surface spline at $t = 1000\tau$ and $N = 100$ with equally spaced nodes.

Example 2. Consider the Allen–Cahn equation with the following initial and boundary conditions

$$\begin{cases} \dfrac{\partial v}{\partial t} - \Delta v + \dfrac{1}{\eta^2}(v^3 - v) = f, \quad (x, y) \in (-1, 1)^2,\ t > 0, \\ v\left(\pm 1, y, t\right) = e^{-\pi} \sin\left((y^2 - 1)t\right),\ v\left(x, \pm 1, t\right) = 0,\ t > 0, \\ v\left(x, y, 0\right) = 0, \quad (x, y) \in [-1, 1]^2, \end{cases}$$

where $\eta = 100$, the exact solution is $v\left(x, y, t\right) = e^{-\pi x^2} \sin\left(\left(y^2 - 1\right) t\right)$ and the right-hand side function f can be computed accordingly.

The comparison of errors for two types of nodes is presented in Table 5, and the plot of the absolute error is given in Figure 5. We also plot the

contour of the error in Figure 6. The obtained errors for this example, by using different time steps, are also presented in Table 6.

Table 5: The comparison of errors of Example 2 for $t = 1000\tau$ by using scattered and equally spaced nodes where time step is $\tau = 10^{-4}$.

Equally Spaced			Scattered	
N	$\|u - u_N\|_\infty$	$\|u - u_N\|_2$	$\|u - u_N\|_\infty$	$\|u - u_N\|_2$
49	$1.07720E-5$	$3.00790E-5$	$1.31170E-5$	$3.15498E-5$
64	$8.74748E-6$	$2.65163E-5$	$1.14132E-5$	$3.47482E-5$
81	$1.67367E-6$	$4.61698E-6$	$1.55723E-6$	$4.72437E-6$
100	$1.33128E-6$	$4.66584E-6$	$1.43747E-6$	$5.21502E-6$
121	$6.75815E-7$	$2.56911E-6$	$7.37549E-7$	$1.53253E-6$
144	$6.28635E-7$	$2.73066E-6$	$5.62016E-7$	$1.69418E-6$

Table 6: The comparison of errors of Example 2 by using various time steps at $N = 100$ and $t = 1000\tau$.

Equally Spaced			Scattered	
Time Step ($\tau = 10^{-4}$)	$\|u - u_N\|_\infty$	$\|u - u_N\|_2$	$\|u - u_N\|_\infty$	$\|u - u_N\|_2$
τ	$1.33128E-6$	$4.66584E-6$	$1.43747E-6$	$5.21502E-6$
$1/2 \times \tau$	$3.29225E-7$	$1.12282E-6$	$3.27643E-7$	$1.21081E-6$
$1/4 \times \tau$	$8.18399E-8$	$2.75750E-7$	$7.82939E-8$	$2.92148E-7$
$1/8 \times \tau$	$2.04010E-8$	$6.83517E-8$	$1.91410E-8$	$7.17766E-8$
$1/16 \times \tau$	$5.09283E-9$	$1.70169E-8$	$4.73236E-9$	$1.77901E-8$

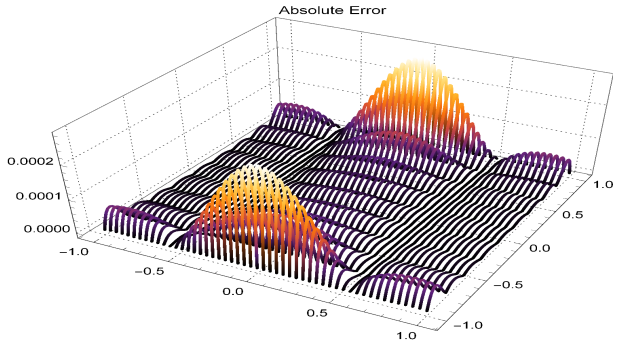

Figure 5: The plot of the error in Example 2, at $t = 1000\tau$ and $N = 100$ for equally spaced nodes.

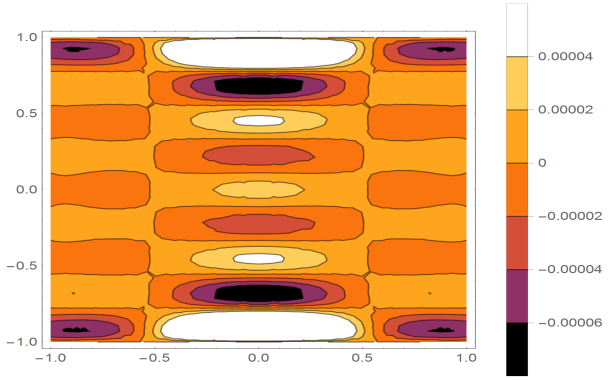

Figure 6: The contour plot of the error in Example 2, at $t = 1000\tau$ and $N = 100$ with equally spaced nodes.

Example 3. For this example, consider the following equation:

$$\begin{cases} \dfrac{\partial v}{\partial t} - \Delta v + \dfrac{1}{\eta^2}(v^3 - v) = f, \ \ (x, y) \in (-1, 1)^2, \ t > 0, \\ v\,(\pm 1, y, t) = 0, \ v\,(x, \pm 1, t) = 0, \ t > 0, \\ v\,(x, y, 0) = \sin(\pi y)\cos(\pi x/2), \ \ (x, y) \in [-1, 1]^2, \end{cases} \tag{11}$$

where $\eta = 100$ and the exact solution is $v\,(x, y, t) = \sin(\pi y)\cos(\pi x/2)\,(1 + t)$ and the function f can be computed accordingly.

The comparison of errors for the equally spaced and the scattered nodes for this example is shown in Table 7. As we expected, better results are obtained for equally spaced nodes. The plot of absolute error, in the case of equally spaced nodes, is presented in Figure 7, and the contour plot of the error is given in Figure 8. In Table 8, the comparison of errors for two types of nodes, by using different time steps is shown.

Table 7: The comparison of errors of Example 3, at $t = 1000\tau$ by using scattered and equally spaced nodes where time step is $\tau = 10^{-4}$.

	Equally Spaced		Scattered	
N	$\|u - u_N\|_\infty$	$\|u - u_N\|_2$	$\|u - u_N\|_\infty$	$\|u - u_N\|_2$
49	$3.07732E-3$	$6.27540E-3$	$5.39392E-3$	$7.59093E-3$
64	$5.49423E-4$	$1.12731E-3$	$1.08340E-3$	$1.38534E-3$
81	$3.37897E-4$	$8.97249E-4$	$6.02756E-4$	$1.14500E-3$
100	$5.51337E-5$	$1.40970E-4$	$1.58731E-4$	$2.24005E-4$
121	$3.34659E-5$	$1.06018E-4$	$4.93030E-5$	$1.29525E-4$
144	$5.23636E-6$	$1.69188E-5$	$1.28415E-5$	$2.64670E-5$

Table 8: The comparison of errors of Example 3, by using various time steps at $N = 100$ and $t = 1000\tau$.

	Equally Spaced		Scattered	
Time Step ($\tau = 10^{-4}$)	$\|u - u_N\|_\infty$	$\|u - u_N\|_2$	$\|u - u_N\|_\infty$	$\|u - u_N\|_2$
τ	$5.51337E-5$	$1.40970E-4$	$1.58731E-4$	$2.24005E-4$
$1/2 \times \tau$	$2.72150E-5$	$6.72841E-5$	$6.89102E-5$	$1.04333E-4$
$1/4 \times \tau$	$1.34159E-6$	$3.27630E-5$	$3.20549E-5$	$5.04380E-5$
$1/8 \times \tau$	$6.65022E-6$	$1.61537E-5$	$1.54562E-5$	$2.48065E-5$
$1/16 \times \tau$	$3.30963E-6$	$8.01907E-6$	$7.58896E-6$	$1.23023E-5$

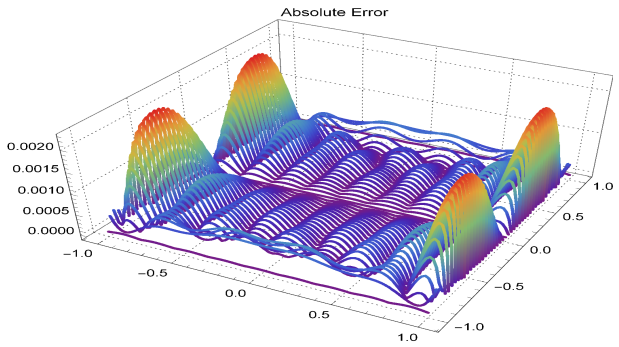

Figure 7: The plot of the error in Example 3, at $t = 1000\tau$ and $N = 100$ with equally spaced nodes.

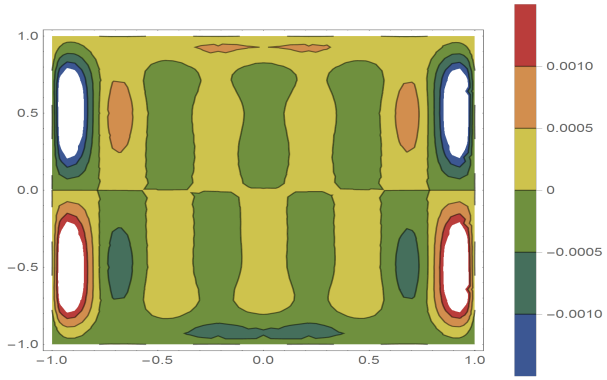

Figure 8: The contour plot of the error in Example 3, at $t = 1000\tau$ and $N = 100$ with equally spaced nodes.

Example 4. For the final example, we solve the following equation in a polygonal domain.

$$\begin{cases} \dfrac{\partial v}{\partial t} - \Delta v + \dfrac{1}{\eta^2}(v^3 - v) = f, \ \ (x,y) \in (-1,1)^2,\ t > 0, \\ v\left(\pm 1, y, t\right) = 0,\ v\left(x, \pm 1, t\right) = 0,\ t > 0, \\ v\left(x, y, 0\right) = \left(x^2 - 1\right)\left(y^2 - 1\right),\ \ (x,y) \in [-1,1]^2, \end{cases} \tag{12}$$

where $\eta = 100$, the exact solution is $v\left(x,y,t\right) = \left(x^2-1\right)\left(y^2-1\right)e^{-\pi^2 t}$ and the function f is computed accordingly.

In this example, for showing the flexibility of our method, we consider a polygonal domain with the following vertices that are arranged in clockwise order:

$$\left\{(-1,1)\,,\,(-1,0)\,,\,(-0.286,0)\,,(0.5,1)\,,(1,1)\,,(1,-1)\right\}.$$

Figure 9 shows the shape of the domain and equally spaced points. As before, the comparison of errors for the equally spaced and the scattered nodes is presented in Table 9. we also plot the absolute error in Figure 10 and the contour plot of the error in Figure 11.

Table 9: The comparison of errors of Example 4, by using various time steps at $N = 165$ and $t = 1000\tau$.

	Equally Spaced		Scattered	
Time Step ($\tau = 10^{-4}$)	$\|u - u_N\|_\infty$	$\|u - u_N\|_2$	$\|u - u_N\|_\infty$	$\|u - u_N\|_2$
τ	$3.20101E-4$	$1.48746E-3$	$3.69452E-4$	$1.00703E-3$
$1/2 \times \tau$	$1.03216E-4$	$4.58850E-4$	$1.49190E-4$	$3.25760E-4$
$1/4 \times \tau$	$3.15830E-5$	$1.28779E-4$	$6.47536E-5$	$1.11007E-4$
$1/8 \times \tau$	$9.89283E-6$	$3.56560E-5$	$3.01340E-5$	$4.73288E-5$
$1/16 \times \tau$	$3.35178E-6$	$1.11966E-5$	$1.45773E-5$	$2.35022E-5$

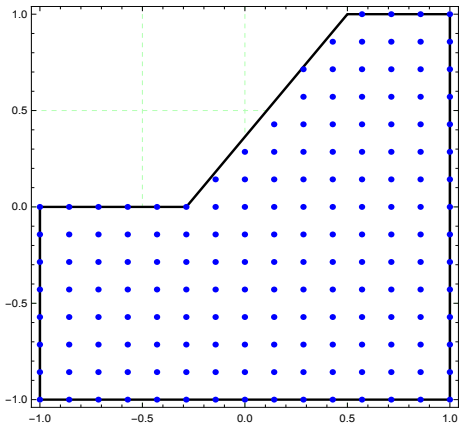

Figure 9: Polygonal domain including 165 equally spaced points for Example 4.

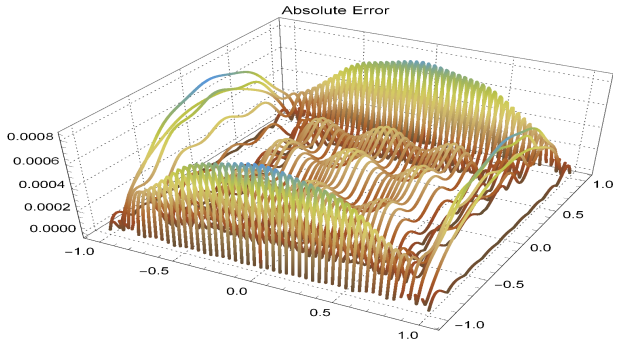

Figure 10: The plot of the error in Example 4, at $t = 1000\tau$ and $N = 100$ with equally spaced nodes.

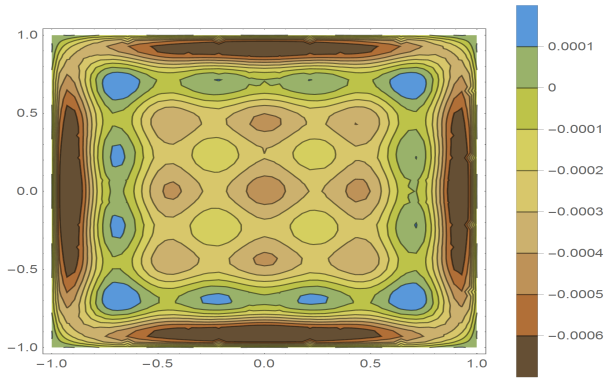

Figure 11: The contour plot of the error in Example 4, at $t = 1000\tau$ and $N = 100$ with equally spaced nodes.

5 Conclusion

In this paper, a fully-discrete approximation of the Allen–Cahn equation was considered. Based on the forward Euler/Crank–Nicolson scheme (in time) and the RBF collocation method (in space), we proposed a numerical scheme, in which the nonlinear term could be treated explicitly and the resultant numerical scheme was linear and easy to implement. Numerical solvability and stability of the method, by using second order finite difference matrices were discussed. Four numerical test problems were considered, which showed the efficiency and reliability of the proposed method. The obtained numerical

results showed that the equally spaced nodes are better in comparison with scattered nodes.

Acknowledgements

The authors would like to thank the anonymous referees for their valuable comments and suggestions, that greatly improved the final version of this article.

References

1. Allen, S.M. and Cahn, J.W. *A microscopic theory for antiphase boundary motion and its application to antiphase domain coarsening,* Acta Metall. 27 (1979) 1085–1095.

2. Bartels, S. *Numerical methods for nonlinear partial differential equations,* Springer Series in Computational Mathematics, vol. 47, Springer, 2015.

3. Buhmann, M.D. *Radial basis functions: Theory and implementations,* Cambridge University Press, Cambridge, 2004.

4. Carr, J.C., Fright, W.R. and Beatson, R.K.*Surface interpolation with radial basis functions for medical imaging,* IEEE Trans. Med. Imaging 16 (1997) 96–107.

5. Cecil, T., Qian, J. and Osher, S. *Numerical methods for high dimensional Hamilton-Jacobi equations using radial basis functions,* J. Comput. Phys. 196 (2004) 327–347.

6. Cheng, A.H.D., Golberg, M.A., Kansa, E.j. and Zammito, G. *Exponential convergence and h-c multiquadric collocation method for partial differential equations,* Numer. Meth. Part. Differ. Equ. 19 (2003) 571–594.

7. Cheng, M. and Warren, J.A. *An efficient algorithm for solving the phase field crystal model,* J. Comput. Phys. 227 (2008) 6241–6248.

8. Fasshauer, G.E. *Meshfree approximation methods with MATLAB*, World Scientific, Hackensack, 2007.

9. Feng, X., Li, Y. and Zhang, Y.*Finite element methods for the stochastics Allen–Cahn equation with gradient-type multiplicative noise,* SIAM J. Numer. Anal. 55(1) (2017) 194–216.

10. Franke, R. *Scattered data interpolation: tests of some methods,* Math. Comput. 38 (1982) 181–200.

11. Hon, Y.C. and Mao, X.Z. *A radial basis function method for solving options pricing model,* Financial Eng. 8 (1) (1999) 31–50.

12. Kessler, D., Nochetto, R. and Schmidt, A. *A posteriori error control for the Allen–Cahn problem: circumventing Gronwall's inequality,* M2AN Math. Model. Numer. Anal. 38 (2004) 129–142.

13. Kim, J., Jeong, D., Yang, S. and Choi, Y. *A finite difference method for a conservative Allen–Cahn equation on non-flat surfaces,* J. Comput. Phys. 334 (2017) 170–181.

14. Kufner, A. and Persson, L.E. *Weighted inequalities of Hardy type,* World Scientific Publishing Co., Inc., River Edge, NJ, 2003.

15. Lee, H. and Lee, J. *A semi-analytical Fourier spectral method for the Allen–Cahn equation,* Comput. Math. Appl. 68 (3) (2014) 174–184.

16. Madych, W.R. and Nelson, S.A. *Multivariable interpolation and conditionally positive definite functions II,* Math. Comput. 54 (1990) 211–230.

17. Mohammadi, V., Mirzaei, D. and Dehghan, M. *Numerical simulation and error estimation of the time-dependent Allen–Cahn equation on surfaces with radial basis functions,* J. Sci. Comput. 79 (2019) 493–516.

18. Park, J. and Sandberg, I.W. *Universal approximations using radial-basis-function networks,* Neu. Comput. 3 (1991) 246–257.

19. Pham, H. *Handbook of engineering statistics,* Springer, 2006.

20. Shen, J., Tang, T. and Wang, L.L. *Spectral methods: Algorithms, analysis and applications,* Springer-Verlag, Berlin, 2011.

21. Shu, C. and Ding, H. *Numerical comparison of least square based finite difference (LSFD) and local multiquadric-differential quadrature (LMQDQ) methods,* Comput. Math. Appl. (submitted).

22. Shu, C., and Ding, H. and Yeo, K.S. *Local radial basis function-based differential quadrature method and its application to solve two-dimensional incompressible N Navier-Stokes equations,* Comput. Methods Appl. Mech. Eng. 192 (2003) 941–954.

23. Sarra, S.A. *A local radial basis function method for advection-diffusion-reaction equations on complexly shaped domains,* Appl. Math. Comput. 218, 19 (2012) 9853–9865.

24. Tolstykh, A.I., Lipavskii, M.V. and Shirobokov, D.A. *High-accuracy discretization methods for solid mechanics,* Arch. Mech. 55 (2003) 531–553.

25. Wright, G.B. and Fornberg, B. *Scattered node compact finite difference-type formulas generated from radial basis functions,* J. Comput. Phys. 212 (2006) 99–123.

26. Wendland, H.*Scattered data approximations*, Cambridge Monographs on Applied Computational Mathematics, Cambridge University Press, 2005.

27. Wu, X., Zwieten, G.J. and Zee, K.G. *Stabilized second-order convex splitting schemes for Cahn-Hilliard models with application to diffuse-interface tumor-growth models,* Int. J. Numer. Methods Biomed. Eng. 30 (2014)180–203.

28. Yoon, J.*Spectral approximation order of radial basis function interpolation on the Sobolev space,* SIAM J. Math. Anal. 33 (2001) 946–958.

29. Yoon, J. *Lp-error estimates for "shifted" surface spline interpolation on Sobolev Space,* Math. Comput. 72 (243) (2003) 1349 –1367.

30. Yoon, J. *Improved accuracy of Lp-approximation to derivatives by radial basis function interpolation,* Appl. Math. Comput. 161 (2005) 109–119.

31. Zhang, J. and Du, Q. *Numerical studies of discrete approximations to the Allen–Cahn equation in the sharp interface limit,* SIAM J. Sci. Comput. 31 (4) (2009) 3042–3063.